Physical speciation of iron in the Atlantic sector of the Southern Ocean along a transect from the subtropical domain to the Weddell Sea Gyre.

Fanny Chever, Eva Bucciarelli, Géraldine Sarthou, Sabrina Speich, Michel Arhan, Pierrick Penven, Alessandro Tagliabue

Physical speciation of iron in the Atlantic sector of the Southern Ocean along a transect from the subtropical domain to the Weddell Sea Gyre

F. Chever,[1,2] E. Bucciarelli,[1,2] G. Sarthou,[1,2] S. Speich,[3] M. Arhan,[3] P. Penven,[3] and A. Tagliabue[4,5]

Received 6 October 2009; revised 23 June 2010; accepted 28 June 2010; published 30 October 2010.

[1] Distributions of total dissolvable iron (TDFe; unfiltered), dissolved iron (DFe; 0.2 μm filtered), and soluble iron (SFe; 0.02 μm filtered) were investigated during the BONUS-GoodHope cruise in the Atlantic sector of the Southern Ocean (34°S/17°E–57°S/0°, February–March 2008). In the mixed layer, mean values of 0.43 ± 0.28 and 0.22 ± 0.18 nmol L^{-1} were measured for TDFe and DFe, respectively. In deeper waters, TDFe and DFe concentrations were 1.07 ± 0.68 and 0.52 ± 0.30 nmol L^{-1}, respectively. DFe concentrations decreased from the north (subtropical waters) to the south (Weddell Sea Gyre). In the subtropical domain, dusts coming from Patagonia and southern Africa and inputs from the African continental margin may explain high DFe and TDFe concentrations in surface and intermediate waters. Results from numerical models gave support to these hypotheses. In the Antarctic Circumpolar Current domain, estimation of the median advective time of water masses suggests that sediment inputs from the Antarctic Peninsula, South America margin, and/or South Georgia Islands could be an important source of Fe. Except in the subtropical domain where 0.4–0.6 nmol L^{-1} of SFe were observed in the upper 1500 m, all stations exhibited values close to 0.1–0.2 nmol L^{-1} in surface and 0.3–0.5 nmol L^{-1} in deeper waters. For all stations, colloidal Fe (CFe) was a minor fraction of DFe in surface waters and increased with depth. Colloidal aggregation, sinking of CFe, and assimilation of SFe, followed by rapid exchange between the two fractions, are suspected to occur.

Citation: Chever, F., E. Bucciarelli, G. Sarthou, S. Speich, M. Arhan, P. Penven, and A. Tagliabue (2010), Physical speciation of iron in the Atlantic sector of the Southern Ocean along a transect from the subtropical domain to the Weddell Sea Gyre, *J. Geophys. Res.*, *115*, C10059, doi:10.1029/2009JC005880.

1. Introduction

[2] The Southern Ocean is the largest high-nutrient low-chlorophyll (HNLC) area of the world ocean, characterized by low primary production along with excess nitrate. Since pioneering work by *Martin et al.* [1990], the pivotal role of iron (Fe) in such marine ecosystems has been demonstrated. This element, exhibiting very low concentrations in surface waters of the HNLC regimes (<0.1 nmol L^{-1}), is an essential nutrient for all marine organisms, playing an important role in many biochemical reactions such as photosynthesis and nitrate reduction [e.g., *Sunda*, 1988–1989]. In situ and natural Fe fertilizations in the Southern Ocean have demonstrated that Fe inputs enhance phytoplankton biomass and affect the major biogeochemical cycles (e.g., carbon (C) and nitrogen (N)) [*Coale et al.*, 2004; *Boyd et al.*, 2000, 2007; *Blain et al.*, 2007; *Pollard et al.*, 2009].

[3] The importance of new sources of Fe to the water column as well as the fractions that are truly bioavailable to the phytoplankton is still a question of debate. Atmospheric deposition was commonly thought to be the predominant external source of Fe in remote areas [*Jickells et al.*, 2005]. However, some studies have shown that inputs from sediments followed by upwelling or advection could provide important supply of Fe in surface waters of the open ocean [*Bucciarelli et al.*, 2001; *Elrod et al.*, 2004; *Lam and Bishop*, 2008; *Tagliabue et al.*, 2009a]. In the deep ocean, hydrothermal inputs could locally increase Fe concentrations [*Boyle and Jenkins*, 2008; *Bennett et al.*, 2008; *Tagliabue et al.*, 2010]. Finally, although considered as a minor source, iceberg melting could also supply Fe to surface waters [*Löscher et al.*, 1997; *Sedwick and DiTullio*, 1997; *Smith et al.*, 2007; *Lancelot et al.*, 2009].

[4] Most of the Fe supplied is present in the particulate pool (>0.2 μm [*de Baar and de Jong*, 2001]). Acidified unfiltered samples (total dissolvable iron (TDFe)) permit the study of the "labile" particulate pool that dissolves during acid storage

[1]Université Européenne de Bretagne, Bretagne, France.
[2]LEMAR, UMR 6539, Université de Brest, CNRS, IRD, UBO, IUEM, Technopôle Brest Iroise, Plouzane, France.
[3]Laboratoire de Physique des Océans, UMR 6523, IFREMER, CNRS, IRD, UBO, Plouzane, France.
[4]LSCE, UMR 1572, IPSL, CEA, CNRS, UVSQ, Gif-sur-Yvette, France.
[5]LOCEAN, UMR 7159, IPSL, UPMC, MHNH, IRD, CNRS, Paris, France.

0148-0227/10/2009JC005880

[*Löscher et al.*, 1997] and gives information on the sources and distribution of iron in seawater [*Chever et al.*, 2010]. More than 99% of dissolved iron (DFe), which passes through an 0.2 or 0.4 μm filter, is complexed by organic ligands [*Gledhill and van den Berg*, 1994; *Rue and Bruland*, 1995], preventing Fe from precipitation and removal by scavenging. The dissolved pool comprises colloidal Fe (CFe; 0.02–0.2 μm) and soluble Fe (SFe; <0.02 μm). The distribution of iron between these two pools (colloidal and soluble) appears related to the distribution of organic ligands that also exist as colloidal and soluble [*Wu et al.*, 2001]. Only a few studies have examined the soluble fraction of Fe, which exhibits nutrient-type profiles, suggesting that this is the bioavailable fraction [*Wu et al.*, 2001; *Bergquist et al.*, 2007]. However, although some studies demonstrated that SFe is more available, CFe can also be a source of Fe to phytoplankton [*Chen and Wang*, 2001; *Chen et al.*, 2003]. The distribution of these two pools of iron needs to be better investigated to further understand the biogeochemical cycle of Fe and its impact on phytoplankton and the C cycle.

[5] In this work, the distributions of DFe, TDFe, and SFe are studied along the BONUS-GoodHope transect, in the Atlantic sector of the Southern Ocean. This transect, from 34°S to 57°S, crossed contrasting oceanographic provinces from the subtropical waters of the southeast Atlantic Ocean to the eastern part of the Weddell Sea Gyre. We will discuss (1) the potential sources of DFe and TDFe in the different domains and (2) the distributions of SFe and CFe in the water column.

2. Materials and Methods

2.1. Study Area

[6] The BONUS-GoodHope cruise took place onboard the R/V Marion Dufresne in the Atlantic sector of the Southern Ocean from 8 February to 24 March 2008. Stations were sampled from the shelf region near Cape Town to 57°33′S along the Greenwich meridian. Figure 1 shows the main oceanographic fronts and domains crossed during the cruise, from north to south: (1) the subtropical domain and the southern subtropical front (S-STF), (2) the Antarctic Circumpolar Current (ACC) domain and its three major fronts (the sub-Antarctic front (SAF), the polar front (PF), and the southern ACC front (SACCF)), and (3) the eastern part of the Weddell Sea Gyre with the southern boundary (SBdy) separating this domain from the ACC.

[7] Twelve stations were sampled for total dissolvable iron (unfiltered iron), dissolved iron (<0.2 μm), and soluble iron (<0.02 μm). Among these stations, seven were sampled between 0 and 2000 m (large stations L1–L7), and five were sampled between 0 and 4000 m (super stations S1–S5). The position of each station is reported in Figure 1 and Table 1 along with the depth of the mixed layer (ML).

2.2. Sampling and Analyses

[8] Samples were collected with acid-cleaned 12 L Go-Flo bottles mounted on a Kevlar cable and tripped by a Teflon messenger, using trace metal clean protocols [*Bruland et al.*, 1979]. Sampling was performed in a clean container. All samples were collected in 60 ml acid-washed low-density polyethylene bottles. TDFe samples were collected without any filtration. Go-Flo bottles were then pressurized with high-purity nitrogen allowing online filtration of seawater through 0.2 μm filter cartridges (SARTOBRAN® 300, Sartorius) for DFe sampling. Soluble samples were obtained by immediate ultrafiltration of DFe on 0.02 μm filters (ANOTOP 25®), which were previously acid cleaned with 10% Suprapur® hydrochloric acid (HCl; Merck) for 10 min and rinsed with milli-Q water for 5 min. This cleaning protocol avoids contamination of the SFe samples. However, we did not test other filters/membranes, and the soluble fraction that we present in this study is thus an operationally defined fraction, using the ANOTOP 25® aluminum oxide membrane. This needs to be taken into consideration when comparing our results to studies using other ultrafiltration methods.

[9] All samples were acidified with Ultrapur® HCl (Merck; 0.2% in volume for TDFe, final pH 1.7; 0.1% in volume for DFe and SFe, final pH 2.2). Samples were stored at room temperature and analyzed at the shore-based laboratory (LEMAR, Brest, France). Given that DFe samples were analyzed at the laboratory more than 2 months after sampling, we assume that the dissolved fraction represents the soluble fraction (SFe) plus the colloids that dissolved during acid storage [*Chever et al.*, 2010]. TDFe samples were stored for at least 5 months before analyses to release all but the most refractory particulate Fe species into the dissolved form [*Löscher et al.*, 1997].

[10] Suprapur® ammonium (NH_4OH; Merck) and ammonium acetate buffer purified three times through an 8-HQ resin were added to the samples to increase pH at 4.7, and analyses were performed by flow injection analysis (FIA) with online preconcentration onto 8-HQ resin and chemiluminescence detection [*Obata et al.*, 1993; modified by *Sarthou et al.*, 2003]. The detection limit was 0.015 ± 0.010 nmol L^{-1} (n = 49). The individual contributions to the total blank of Ultrapur® HCl (Merck), Suprapur® NH_4OH (Merck), and ammonium acetate buffer were determined by addition of increasing amounts of these reagents to the sample and were lower than our detection limit. The accuracy of the method was assessed by analyzing the DFe reference materials collected during the SAFe intercomparison cruise (2004). Concentrations were equal to 0.094 ± 0.005 nmol L^{-1} (n = 3) and 0.862 ± 0.017 nmol L^{-1} (n = 3) for surface S1 and deep D2, respectively, in agreement with the certified values of 0.097 ± 0.043 and 0.91 ± 0.17 nmol L^{-1} [*Johnson et al.*, 2007].

3. Results

3.1. Hydrography

[11] *Gladyshev et al.* [2008] provided a description of the water mass arrangement along a track identical to that of the BONUS-GoodHope cruise, using hydrographic measurements performed in 2004. We briefly summarize the essential characters of this hydrological structure here, referring to the salinity section sampled during BONUS-GoodHope (Figure 2) and to the vertical profiles of temperature and salinity at all large and super stations (Figure 3).

[12] The subtropical domain extended southward to the S-STF (about 42°S), this limit being located between L2 and S2. The entire subtropical region is impacted by the Agulhas Current that follows the eastern coast of South Africa and retroflects eastward, forming intense anticyclonic eddies,

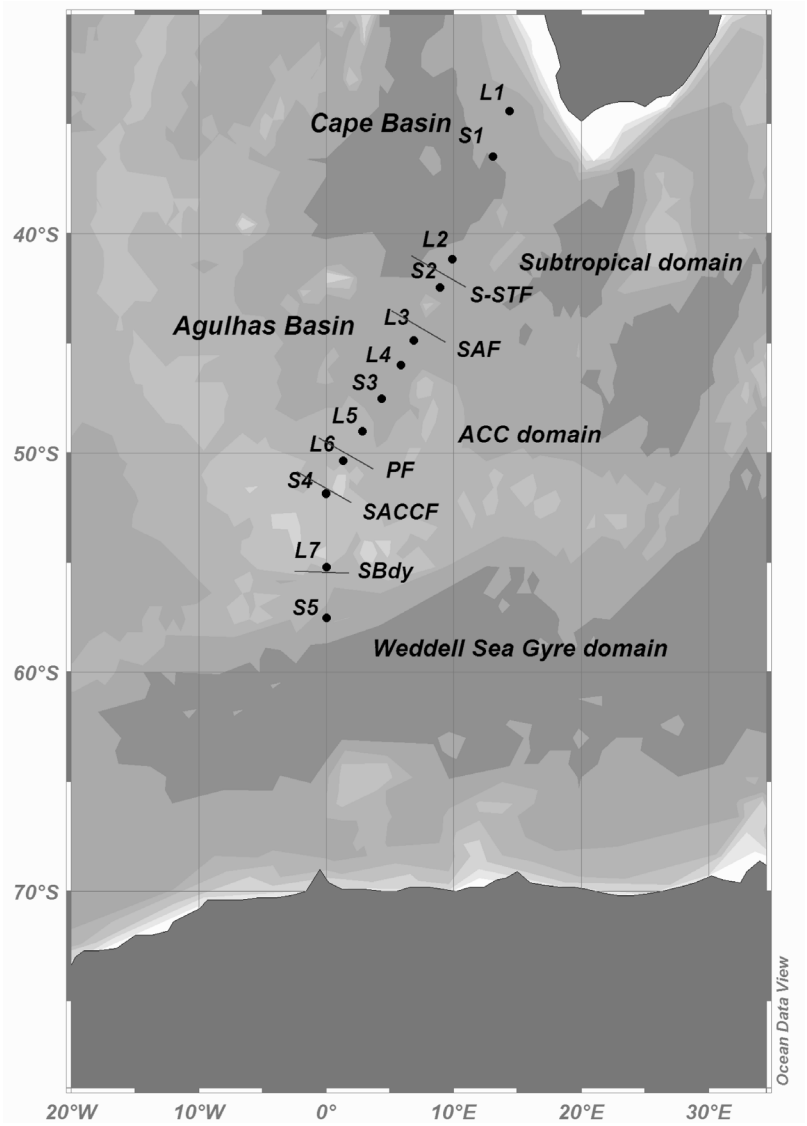

Figure 1. Location of the stations sampled during the BONUS-GoodHope cruise along with the three main oceanographic provinces encountered. The three domains crossed were the subtropical domain (stations L1, S1, and L2), the ACC domain (stations S2, L3, L4, S3, L5, L6, S4, and L7), and the eastern part of the Weddell Sea Gyre (station S5). Five fronts were crossed: the S-STF, SAF, PF, SACCF, and SBdy.

called Agulhas rings [*Lutjeharms and van Ballegooyen*, 1988; *van Ballegooyen et al.*, 1994]. Its central water layer (potential temperature higher than ~10°C, salinity higher than ~34.5) (Figures 2, 3a, and 3b) was mostly occupied by water of Indian Ocean origin [*Boebel et al.*, 2003]. At intermediate depths, two varieties of Antarctic Intermediate Water (AAIW) are generally found in this region [*Gordon et al.*, 1992]. One closer to Africa with a salinity maximum exceeding 34.3 comes from the Indian Ocean through the Agulhas Current. The other one with a salinity maximum lower than 34.3 is formed in the Atlantic sector. The limit separating the two varieties was found near 37°S (south of S1) during the BONUS-GoodHope cruise. Below AAIW, the Upper Circumpolar Deep Water (UCDW) characterized by a core of low oxygen at ~1200 m depth (and not distinguishable in Figure 2) did not show such easily separated varieties, but its northern part was also likely conveyed by the Agulhas Current. Deeper along the subtropical segment of the cruise track, diluted North Atlantic Deep Water (NADW) was characterized by a salinity maximum at 2000–3000 m. The highest salinity values close to the African continental slope reflect advection by a southeastward deep boundary current [*Arhan et al.*, 2003]. The deep-reaching turbulence causes this water mass to spread beyond the Agulhas Ridge. We refer to this variety of NADW as to southeast NADW. Finally, Antarctic Bottom Water (AABW) originating from the Weddell Sea present deeper than ~3500 m in the Cape Basin (Figures 2, 3a, and 3b) is generally thought to circulate cyclonically in this basin [*Reid*, 1989].

[13] Further south, the domain of the ACC extended from the S-STF to the SBdy (~42°S to ~55°S, stations L3–L7). This region is impacted by strong currents of westward origin.

Table 1. Location of the Stations Sampled During the Cruise in Relation to the Domains and Fronts Crossed and Mixed Layer Depth Observed From the Vertical Profile of Temperature for Nearby CTD Station

Oceanographic Domain	Fronts Crossed	Station	Position	ML Depth (m)
Subtropical		L1	34.43°S, 14.40°E	50–60
		S1	36.50°S, 13.10°E	40–50
		L2	41.18°S, 09.92°E	25
	S-STF		42.2°S	
ACC		S2	42.47°S, 08.93°E	50–80
	SAF		44.2°S	
		L3	44.88°S, 06.88°E	60–80
		L4	46.02°S, 05.87°E	80
		S3	47.55°S, 04.37°E	80–100
		L5	49.03°S, 02.84°E	100–110
	PF		50.2°S	
		L6	50.38°S, 01.33°E	60–80
	SACCF		51.5°S	
		S4	51.85°S, 00.00°E	120–150
		L7	55.23°S, 00.03°E	80–110
	SBdy		55.5°S	
Eastern part of the Weddell Sea Gyre		S5	57.55°S, −00.03°E	100

Although station S2 is located south of the S-STF, its surface waters exhibit salinity and temperature signatures of subtropical waters, which suggest an advection from the S-STF region by a neighboring eddy. As S2 otherwise appears like ACC stations in terms of DFe distribution (Figure 4a), it will be discussed in this domain (see section 4.1.2). The SAF and PF were found at ~45°S and 51°S, respectively. Between these two fronts, the water mass with salinity lower than 34.3 was AAIW. It was located beneath the surface mixed layer and winter water (marked by a temperature minimum in Figure 3c). Below AAIW were UCDW, the deep waters visible from their southward shallowing salinity maximum, and the Antarctic Bottom Waters here observed against the northern flank of the Mid-Atlantic Ridge (MAR). *Whitworth and Nowlin* [1987] showed that the deep waters at these latitudes are composed of Lower Circumpolar Deep Water with, north of the PF, an addition of diluted southwest NADW, which flows along the continental slope of South America (Argentinean Basin) before being injected in the ACC in the southwestern Atlantic.

[14] South of the SBdy, and only sampled at S5, were waters entrained in the large-scale cyclonic flow of the Weddell Sea Gyre. The near-surface waters are thought to have been in contact with the western continental margin of the Antarctic Peninsula, while the deeper waters might have had a more recent contact with the northern topographic limit of the Weddell Basin [*Orsi et al.*, 1993; *Meredith et al.*, 2000; *Klatt et al.*, 2005].

3.2. Fe Distributions

[15] Concentrations of DFe, TDFe, and SFe are reported in Table 2. Apparent particulate iron (Fe_{app}), calculated by subtracting DFe from TDFe, is defined as biogenic iron and labile lithogenic particulate Fe, and iron adsorbed on lithogenic or biogenic particles [*de Baar et al.*, 1999]. Mean values of DFe, TDFe, and Fe_{app} in the mixed layer and below the mixed layer are presented in Table 3. The sections of DFe and Fe_{app} are presented in Figure 4. These sections have, however, to be interpreted with caution given the extrapolation caused by the large distance between some stations.

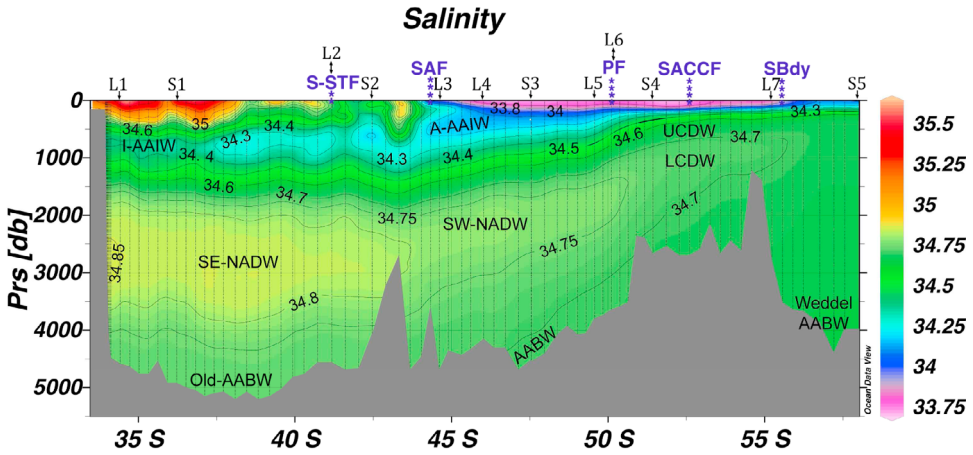

Figure 2. Vertical distribution of salinity (psu) encountered along the transect from the north (left) to the south (right) of the section. Water masses are indicated. I-AAIW, Indian Antarctic Intermediate Water; A-AAIW, Atlantic Antarctic Intermediate Water; SE-NADW, southeast North Atlantic Deep Water; SW-NADW, southwest North Atlantic Deep Water; LCDW, Lower Circumpolar Deep Water.

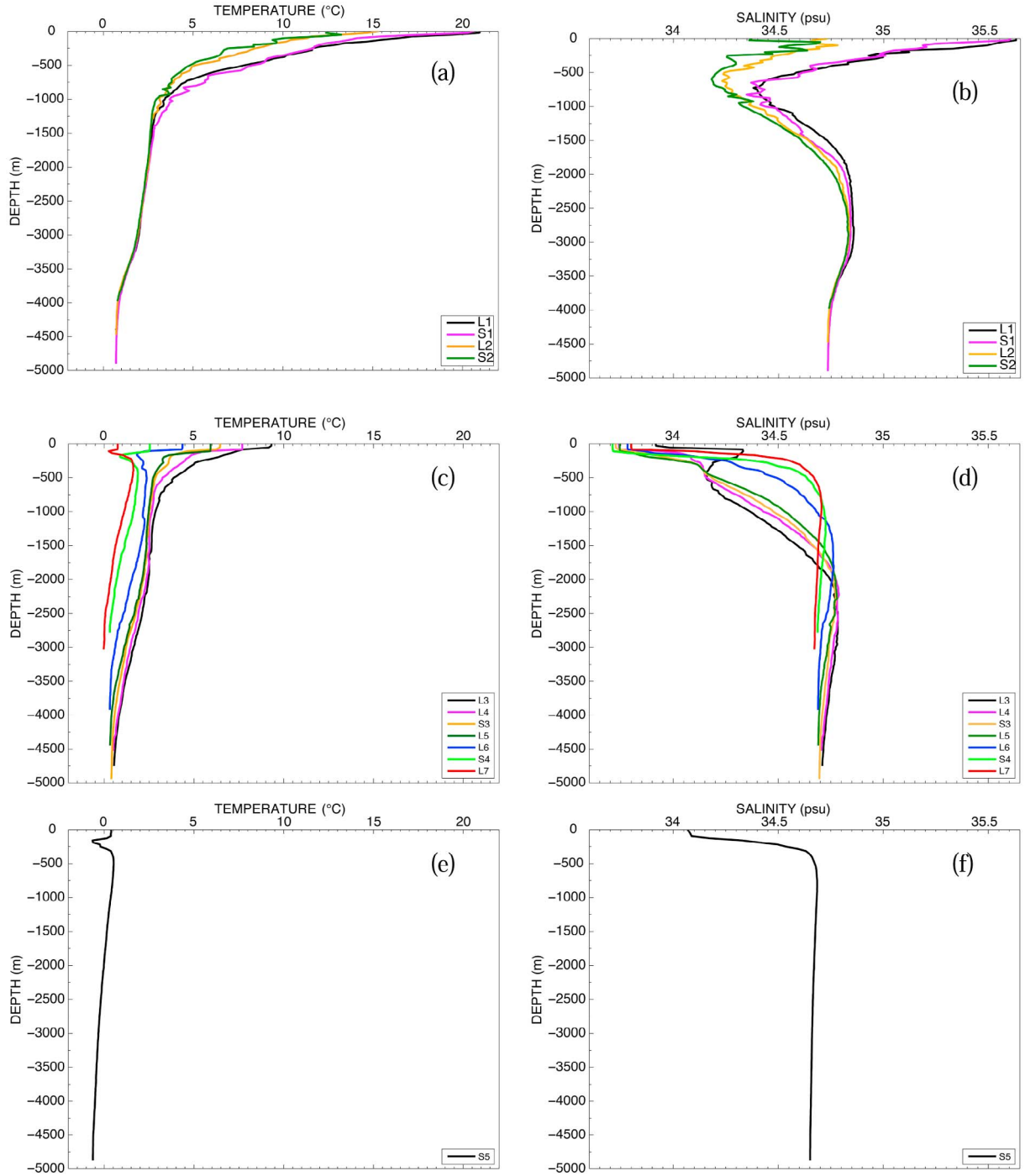

Figure 3. Vertical profiles of potential (a, c, and e) temperature (°C) and (b, d, and f) salinity (psu) in the three different domains. Stations located in the same domain are considered together.

[16] Figure 4a shows a decrease in DFe concentrations from the north to the south of the section. In the ML, values ranged from 0.064 ± 0.006 nmol L^{-1} (L7, 100 m) to 0.720 ± 0.011 nmol L^{-1} (S1, 30 m). Below the ML, values ranged from 0.092 ± 0.004 nmol L^{-1} (L7, 120 m) to 1.583 ± 0.009 nmol L^{-1} (S1, 4000 m).

[17] TDFe values were the lowest in the ACC domain. In the ML, values ranged from 0.191 ± 0.007 nmol L^{-1} (S4, 130 m) to 1.276 ± 0.027 nmol L^{-1} (S5, 60 m). Below the ML, concentrations ranged from 0.234 ± 0.012 nmol L^{-1} (S4, 160 m) to 3.918 ± 0.063 nmol L^{-1} (L1, 2100 m). The section of Fe_{app} is presented in Figure 4b. In the ML, concentrations were low, ranging from 0.025 ± 0.027 nmol L^{-1} (S3, 70 m) to 0.424 ± 0.058 nmol L^{-1} (L1, 20 m), except at the most southerly station (S5) where values were close to 1 nmol L^{-1}. Below the ML, the highest Fe_{app} concentrations were measured in the subtropical domain between 800 and 2100 m, with values ranging from 1.944 ± 0.110 to 3.258 ±

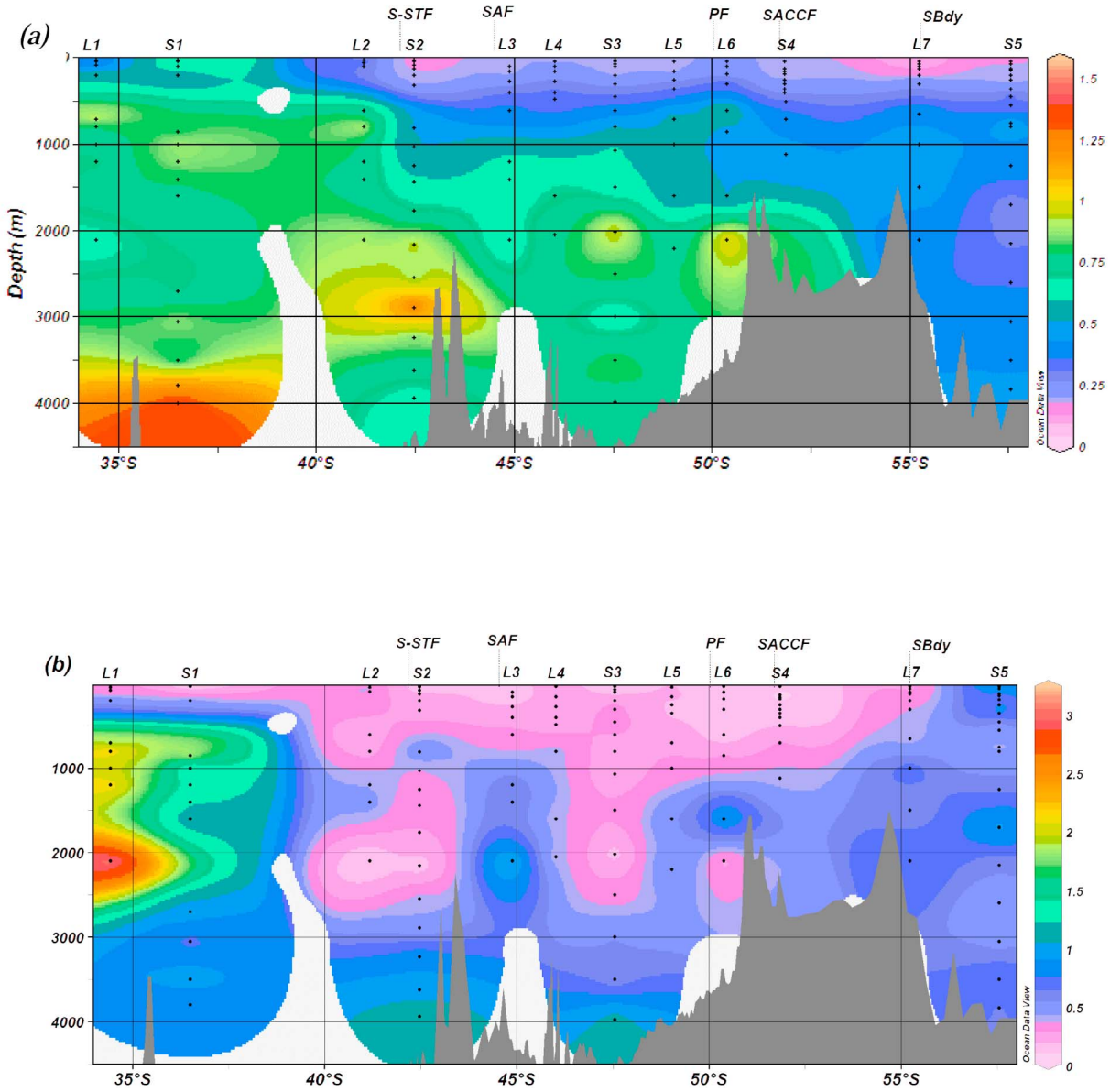

Figure 4. Vertical section of (a) DFe and (b) Fe_{app} concentrations (in nmol L^{-1}) from the north (left) to the south (right) of the section. Note that the concentration scale is not the same.

0.071 nmol L^{-1}. In the ACC and at S5 station, Fe_{app} values varied from 0.026 ± 0.060 nmol L^{-1} (L6, 600 m) to 1.252 ± 0.047 nmol L^{-1} (L3, 2100 m). In the ML, Fe_{app} represented 42 ± 23% (n = 20) of the TDFe except at S5, where it represented 88 ± 1% (n = 29) of the TDFe. Below the ML, Fe_{app} represented 80 ± 4% (n = 4) of the TDFe at the L1 station between 800 and 2100 m, whereas it represented 47 ± 18% (n = 109) in the remaining transect.

[18] Vertical profiles of DFe, SFe, and colloidal Fe (CFe = DFe − SFe) are plotted in Figures 5a–5c for the five super stations. Except at the S1 station where high values of SFe were observed in the upper 1500 m (0.4–0.6 nmol L^{-1}) (Figure 5b), all stations exhibited the same pattern with values close to 0.1–0.2 nmol L^{-1} in surface and 0.3–0.5 nmol L^{-1} in deeper waters. For all stations, CFe was the minor fraction of DFe in surface (i.e., 23 ± 11%, n = 3), but this fraction increased with depth (i.e., 37 ± 21% of the DFe (n = 28) between the ML and 2000 m and 53 ± 15% (n = 16) below 2000 m).

4. Discussion

[19] DFe concentrations observed during BONUS-GoodHope are in the same range as previous values measured in the same sector of the Southern Ocean by *Landing and Powell* [1998] (33°S, 0.5–2.6 nmol L^{-1}) and *de Jong et al.* [1999] (~52°–60°S, 0.05–0.90 nmol L^{-1}). The decrease in concentrations from the north to the south is consistent with a recent study south of Tasmania (SR3 section, between 42°S and 54°S) during fall 1998 [*Sedwick et al.*, 2008]. TDFe concentrations are coherent with values measured in the same sector of the Southern Ocean (6°E, 50°–60°S, 0.18–2.69 nmol L^{-1}) [*Croot et al.*, 2004].

Table 2. DFe, TDFe, and SFe and Location of the Stations[a]

Domain	Station	Position	Bottom Depth (m)	Depth (m)	DFe (nmol L^{-1})	STD (nmol L^{-1})	TDFe (nmol L^{-1})	STD (nmol L^{-1})	SFe (nmol L^{-1})	STD (nmol L^{-1})
Subtropical	L1	34.43°S, 14.40°E	4505	20	0.230	0.008	0.654	0.050		
				40	0.501	0.002	0.678	0.014		
				60	nv		0.547	0.022		
				80	0.211	0.002	0.400	0.012		
				200	0.745	0.002	1.469	0.067		
				700	1.155	0.012	2.740	0.156		
				800	0.639	0.006	3.320	0.109		
				1000	0.656	0.008	2.600	0.102		
				1200	0.633	0.006	3.202	0.174		
				2100	0.660	0.008	3.918	0.063		
	S1	36.50°S, 13.10°E	4915	20	0.700	0.007	0.730	0.012	nv	
				30	0.720	0.011	0.767	0.032	0.525	0.006
				40	nv		0.817	0.015	0.425	0.022
				70	nv		0.575	0.016		
				100	0.815	0.022	nv		nv	
				200	0.364	0.005	0.968	0.040		
				300	nv		2.248	0.074	0.563	0.049
				500	nd		1.971	0.013		
				700	nv		2.727	0.037	0.646	0.010
				850	0.717	0.014	3.185	0.049		
				1000	1.014	0.037	1.369	0.036		
				1200	0.943	0.005	2.380	0.088	0.628	0.007
				1400	0.764	0.010	1.881	0.011		
				1600	0.724	0.112	1.619	0.022	0.366	0.015
				2000	nd		1.728	0.033		
				2700	0.658	0.012	1.621	0.022		
				3050	0.911	0.002	1.536	0.020	0.368	0.003
				3500	0.585	0.005	1.683	0.010		
				3800	1.154	0.011	1.838	0.025	0.448	0.006
				4000	1.583	0.009	nd			
	L2	41.18°S, 09.92°E	4525	15	0.156	0.000	0.293	0.013		
				35	nv		0.349	0.008		
				45	0.590	0.054	1.261	0.012	0.431	0.082
				95	0.291	0.013	0.729	0.021		
				300	nv		0.455	0.011		
				600	0.741	0.010	0.934	0.018		
				800	1.098	0.032	1.265	0.039	0.266	0.004
				1200	0.829	0.008	1.277	0.026		
				1400	0.776	0.024	1.350	0.009		
				2100	0.915	0.040	0.987	0.404		
ACC	S2	42.47°S, 08.93°E	4070	15	0.179	0.013	0.265	0.016	nv	
				30	0.129	0.012	0.284	0.010	nv	
				35	0.098	0.008	0.196	0.008	nv	
				45	nd		nd			
				80	0.152	0.004	0.292	0.004	nv	
				120	0.164	0.005	0.314	0.010	0.162	0.012
				196	0.178	0.005	0.624	0.018	nv	
				314	0.169	0.004	0.412	0.004		
				461	nv		0.604	0.019	0.200	0.009
				598	nv		0.849	0.037		
				809	0.434	0.003	1.123	0.014		
				1029	0.431	0.007	0.736	0.001	0.319	0.004
				1250	0.460	0.006	0.823	0.020	0.364	0.008
				1441	0.641	0.010	0.834	0.016	0.415	0.009
				1764	0.649	0.005	0.950	0.020		
				2156	1.028	0.014	1.069	0.034	0.369	0.005
				2548	0.785	0.014	1.240	0.025	0.378	0.007
				2891	1.459	0.015	1.828	0.048	0.330	0.003
				3234	0.782	0.026	1.714	0.022		
				3626	0.716	0.010	1.687	0.064	0.339	0.006
				3940	0.625	0.008	1.840	0.033		
	L3	44.88°S, 06.88°E	4315	30	nv		0.265	0.019	0.215	0.008
				100	0.205	0.018	0.279	0.010	nv	
				150	0.121	0.011	0.268	0.017	0.097	0.021
				270	0.203	0.005	0.376	0.011		
				400	0.337	0.013	0.651	0.007	0.327	0.021
				600	0.435	0.007	0.759	0.011		
				1200	0.613	0.022	1.248	0.037		
				1400	0.621	0.008	1.283	0.014	0.335	0.012
				2100	0.600	0.002	1.852	0.046	0.339	0.014

Table 2. (continued)

Domain	Station	Position	Bottom Depth (m)	Depth (m)	DFe (nmol L^{-1})	STD (nmol L^{-1})	TDFe (nmol L^{-1})	STD (nmol L^{-1})	SFe (nmol L^{-1})	STD (nmol L^{-1})
	L4	46.02°S, 05.87°E	4147	30	0.165	0.017	0.477	0.069		
				60	nv		0.276	0.003	0.103	0.010
				100	0.208	0.011	0.345	0.022		
				150	0.229	0.013	0.441	0.005		
				270	0.280	0.006	0.582	0.012	0.119	0.001
				400	0.346	0.006	0.487	0.026		
				480	0.381	0.026	0.637	0.010	0.145	0.012
				800	0.331	0.004	0.806	0.028	0.239	0.002
				1600	0.699	0.027	1.034	0.026	0.150	0.002
				2050	0.782	0.019	1.090	0.020	0.236	0.007
	S3	47.55°S, 04.37°E	4480	20	0.161	0.020	0.318	0.016	0.144	0.005
				30	0.170	0.004	0.245	0.015		
				40	nv		0.261	0.013	0.186	0.004
				70	0.185	0.014	0.210	0.013		
				100	0.187	0.021	0.324	0.010		
				200	0.141	0.009	0.629	0.011	0.140	0.004
				300	0.281	0.003	0.636	0.003		
				450	0.286	0.000	0.651	0.048	nv	
				600	0.410	0.011	0.706	0.008		
				800	0.557	0.011	0.735	0.009	0.283	0.029
				1070	0.656	0.014	0.843	0.018	0.268	0.020
				1500	0.600	0.005	0.882	0.012	0.284	0.007
				2020	1.096	0.034	1.156	0.074		
				2500	0.796	0.030	1.102	0.166		
				3000	0.591		1.168	0.077	0.263	0.020
				3500	0.825	0.006	1.345	0.049	0.300	0.002
				3980	0.761	0.017	1.946	0.096	0.340	0.002
	L5	49.03°S, 02.84°E	4025	40	0.141	0.005	0.360	0.034		
				80	nv		0.381	0.284		
				150	0.133	0.001	0.383	0.014		
				170	nv		0.238	0.006	nv	
				250	0.216	0.001	0.356	0.001	nv	
				350	0.354	0.015	0.519	0.018		
				700	0.604	0.012	0.905	0.006		
				1000	0.504	0.003	0.812	0.006	0.425	0.151
				1600	0.473	0.007	1.051	0.027	nv	
				2200	0.722	0.016	1.323	0.014	0.517	0.015
	L6	50.38°S, 01.33°E	3576	30	0.249	0.016	0.275	0.020	nv	
				60	nv		0.300	0.034		
				100	0.217	0.023	0.455	0.016	nv	
				135	nv		0.362	0.013	nv	
				180	0.211	0.009	0.402	0.009		
				300	0.421	0.074	0.598	0.009	0.304	0.020
				600	0.850	0.023	0.876	0.037		
				850	0.449	0.009	0.775	0.013	0.380	0.002
				1600	0.431	0.013	1.470	0.043		
				2100	1.123	0.035	1.260	0.054	0.566	0.017
	S4	51.85°S, 00.00°E	2632	30	0.182	0.004	0.338	0.028	0.128	0.018
				60	nv		0.240	0.011		
				130	0.136	0.008	0.191	0.007	nv	
				160	0.126	0.006	0.234	0.012	nv	
				180	0.184	0.002	0.264	0.007		
				250	0.191	0.005	0.258	0.005	nv	
				300	0.202	0.012	0.309	0.002		
				350	0.203	0.003	0.373	0.008		
				400	0.213	0.005	0.360	0.007	nv	
				500	0.447	0.002	0.708	0.005	0.334	0.015
				700	0.426	0.002	0.792	0.047		
				900	nv		0.546	0.042	0.287	0.008
				1117	0.460	0.003	0.885	0.034		
				1950	nv		0.799	0.022	0.290	0.016
				2300	nv		1.510	0.022	0.335	0.006
				2500	0.787	0.027	1.240	0.021	0.339	0.024
	L7	55.23°S, 00.03°E	2770	30	0.110	0.002	0.381	0.017		
				60	0.065	0.004	0.224	0.021	nv	
				100	0.064	0.006	0.244	0.007		
				120	0.092	0.004	0.549	0.014	nv	
				200	0.212	0.003	0.524	0.007		
				300	0.369	0.003	0.794	0.084		
				650	0.451	0.002	0.810	0.010	nv	

Table 2. (continued)

Domain	Station	Position	Bottom Depth (m)	Depth (m)	DFe (nmol L^{-1})	STD (nmol L^{-1})	TDFe (nmol L^{-1})	STD (nmol L^{-1})	SFe (nmol L^{-1})	STD (nmol L^{-1})
				1000	0.494	0.007	1.239	0.007		
				1500	0.482	0.010	1.044	0.017	0.282	0.014
				2100	0.390	0.009	1.171	0.054	0.326	0.017
Eastern part of the Weddell Sea Gyre	S5	57.55°S, −00.03°E	3932	30	0.145	0.011	1.231	0.031	nv	
				60	0.144	0.001	1.276	0.027		
				120	0.313	0.008	0.894	0.037	0.245	0.021
				140	0.110	0.010	0.637	0.027		
				190	0.133	0.002	0.779	0.006	nv	
				250	0.166	0.005	1.057	0.005	nv	
				350	0.142	0.001	1.303	0.019		
				450	0.517	0.029	0.758	0.014	0.326	0.017
				550	0.161	0.004	0.657	0.024		
				750	0.713	0.040	0.933	0.019	0.268	0.012
				800	0.341	0.005	0.895	0.018		
				1250	0.417	0.007	1.030	0.017	0.214	0.008
				1700	0.259	0.004	1.308	0.081		
				2150	0.290	0.003	0.803	0.013		
				2600	0.365	0.016	0.818	0.108		
				3050	0.418	0.003	0.909	0.033	0.237	0.001
				3500	0.382	0.003	1.174	0.017		
				3840	0.511	0.023	1.121	0.015	0.212	0.016

[a]Uncertainties on the concentrations correspond to standard deviation (SD) of a same sample measured three times. SFe samples were not validated when concentrations were higher than DFe. DFe samples were not validated when concentrations were higher than TDFe. Here nv, not validated; nd, not determined.

[20] Vertical profiles of SFe were rarely studied in the Southern Ocean and were analyzed in geographically restricted areas in the Atlantic Ocean. To our knowledge, only one profile was reported in the Southern Ocean during the EisenEx iron enrichment experiment, outside the iron-fertilized patch (~20°E, 48°S) [*Nishioka et al.*, 2005]. Concentrations were twice lower than those measured in our study, with mean concentrations of 0.04 ± 0.01 nmol L^{-1} ($n = 5$) and 0.16 ± 0.03 nmol L^{-1} ($n = 9$) for surface and deep waters, respectively. In the Pacific and Atlantic Oceans, SFe concentrations were equal to ~0.1 nmol L^{-1} in the surface and to ~0.3–0.4 nmol L^{-1} in deeper water [*Wu et al.*, 2001; *Bergquist et al.*, 2007].

[21] In the surface layer of the North Pacific and Atlantic Oceans, contrary to what we observed, CFe represented the main fraction of DFe (71–90%) [*Nishioka et al.*, 2001; *Wu et al.*, 2001; *Cullen et al.*, 2006]. However, the percentage of CFe was much lower (~35%) during the EisenEx enrichment in the Southern Ocean [*Nishioka et al.*, 2005]. In the deep water, the proportion of CFe relative to DFe observed during our study was similar to values observed in the literature (30–70%) [*Wu et al.*, 2001; *Cullen et al.*, 2006; *Nishioka et al.*, 2005].

4.1. Sources of Iron

4.1.1. Subtropical Domain (Stations L1, S1, and L2)

[22] The atmospheric input is a potential source of Fe in this region. This input is recognized to be temporally and spatially variable with some sporadic strong inputs [*Jickells and Spokes*, 2001]. Several studies suggest that the Patagonian desert could be one of the main sources of dust in the Atlantic sector of the Southern Ocean [*Mahowald et al.*, 1999; *Erickson et al.*, 2003; *Meskhidze et al.*, 2007], with higher dust activity generally observed in the summer period [*Gassó and Stein*, 2007]. The NOAA Hybrid Single-Particle Lagrangian Integrated Trajectory (HYSPLIT) model (http://www.arl.noaa.gov/ready.html) allows us to determine the potential origin of air masses during the cruise at a determined point. This air mass back trajectory model was run for all of the stations at heights of 10, 500, and 1000 m over a 5 day period. Air masses originating from Patagonia were observed during the cruise only at the three subtropical stations (Figure 6). However, this model gives us information on a short time scale (few days). To assess the cumulative aeolian input of DFe over a seasonal time scale (4 months) in the subtropical domain, we used a regional oceanic model based on the Regional Ocean Modelling System (ROMS) (Southern African Experiments (SAfE) [*Penven et al.*, 2006]) forced by two different atmospheric dust products. ROMS-SAfE resolves the complex physics of the region, but this model does not include any DFe loss terms (e.g., scavenging/precipitation or biotic uptake) and should therefore be seen to provide the maximum potential impact of dust Fe on DFe. To account for DFe losses, we also used results of the global ocean biogeochemistry model Pelagic Iteraction Scheme for Carbon and Ecosystem Studies (PISCES) when dust DFe sources were eliminated during equilibrium simulations. PISCES is a lower resolution than ROMS-SAfE but provides an estimate as to the overall importance of different DFe

Table 3. Mean Concentrations of DFe, TDFe, and Fe_{app} in the ML and Below the ML

	Position	Mean Value
DFe (nmol L^{-1})	ML	0.216 ± 0.177 ($n = 23$)
	Below ML	0.521 ± 0.303 ($n = 113$)
TDFe (nmol L^{-1})	ML	0.430 ± 0.283 ($n = 31$)
	Below ML	1.066 ± 0.684 ($n = 127$)
Fe_{app} (nmol L^{-1})	ML	0.234 ± 0.300 ($n = 22$)
	Below ML	0.559 ± 0.551 ($n = 113$)

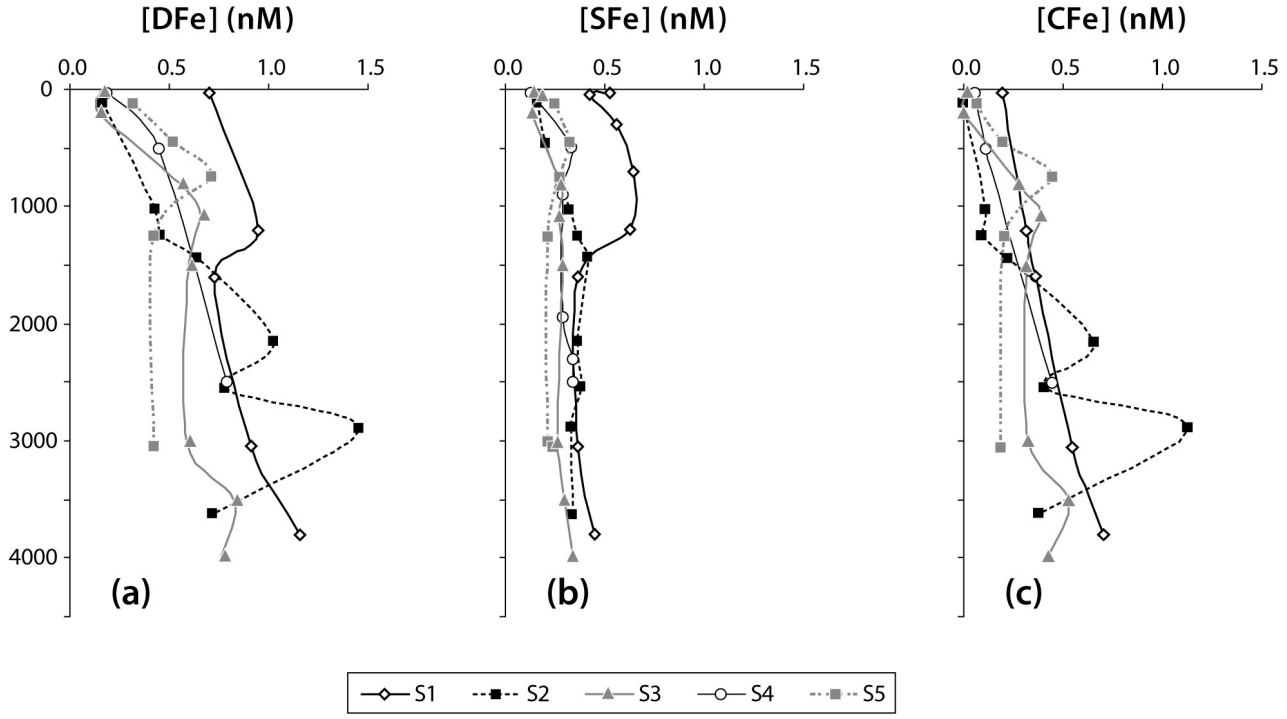

Figure 5. Vertical profiles of (a) DFe, (b) SFe, and (c) CFe (in nmol L^{-1}) at the five super stations.

sources when the iron cycle is accounted for [*Tagliabue et al.*, 2009a]. We used two different estimates of atmospheric dust input to the ocean. The first is the National Center for Atmospheric Research (NCAR) model [*Mahowald et al.*, 2006], which has a large Patagonian dust source (~20 mg m^{-2} $month^{-1}$ close to Patagonia, 2–10 mg m^{-2} $month^{-1}$ around southern Africa, and 2–5 mg m^{-2} $month^{-1}$ along the cruise transect in the subtropical domain). The second is the Integrated Catchment Model (INCA) model [*Aumont et al.*, 2008], which has a reduced Patagonian source but a greater source from southern Africa (<2 mg m^{-2} $month^{-1}$ close to Patagonia, 2–50 mg m^{-2} $month^{-1}$ around southern Africa, and ~2 mg m^{-2} $month^{-1}$ along the cruise transect in the subtropical domain). A Fe content of 3.5% [*Desboeufs et al.*, 2005] and a solubility of 5% [*Baker et al.*, 2006] and 10% [*Duce and Tindale*, 1991] were applied to each dust model for study with ROMS-SAfE (PISCES simulations used their typical experimental design [see *Tagliabue et al.*, 2009a]). The solubility of 10% used with ROMS-SAfE also agrees with the average value of 10.3% calculated for samples collected in the South Atlantic south of 35°S (A. Baker, personal communication, 2010).

[23] Using NCAR, ROMS-SAfE suggests that at the two groups of stations (L1/S1 and L2), dust deposition from Patagonia could be a significant source of DFe (up to ~0.6 nmol L^{-1} after 4 months) (Figure 7b, dotted lines). Similarly, the results from PISCES suggest that up to 0.2 nmol L^{-1} of DFe at these stations was maintained by dust deposition from Patagonia at steady state. However, stations L1, S1, and L2 might also have been enriched by atmospheric dust inputs from southern Africa, followed by lateral advection. Indeed, major transport pathways of air masses over southern Africa are from the interior of the continent toward the Indian Ocean [*Piketh et al.*, 2002]. Experiments with ROMS-SAfE using INCA dust deposition showed that at L1 and S1 stations, the maximum potential enrichment was around 0.15 or 0.3 nmol L^{-1} after 4 months, using 5% or 10% of solubility, respectively (Figures 7a and 7b, solid line). Analyzed more in detail, the model results revealed that the increase of 0.15–0.3 nmol L^{-1} was mainly controlled by the advection of Indian Ocean waters (data not shown). At the L2 station, there was no significant advection of Indian Ocean waters (increase in DFe < 0.05 nmol L^{-1} after 4 months) (Figures 7a and 7b, dotted line), suggesting that only direct dust deposition coming from Patagonia is likely to increase DFe in surface waters at this station. In accord, under INCA dust forcing, PISCES suggests that dust contributes 0.1 nmol L^{-1} to DFe at L1 and S1, with a contribution of <0.05 nmol L^{-1} at L2.

[24] Another potential source of Fe to the subtropical region is the continental margin. Indeed, the surface waters of the Cape Basin from Indian Ocean origin might also have been enriched by Fe when they swept the African continental margin. Previous work in the Southern Ocean already mentioned regions impacted by advection of water masses that have been in contact with continental shelves [*Sedwick et al.*, 1997]. The transit time of the water masses between the southeast Indian Ocean (30°S) and the BONUS-GoodHope transect was estimated from the Archiving, Validation, and Interpretation of Satellite Oceanographic Mean Absolute Dynamic Topography [*Ducet et al.*, 2000] for both the specific cruise period (2007–2008) and for the entire satellite time series (i.e., from 1992 to 2008). It gave an estimate for the mean advective time between 1 and 3 months. Given that the residence time of Fe in surface water is on the order of days to months [*de Baar and de Jong*, 2001; *Croot et al.*, 2004; *Sarthou et al.*, 2003], Fe transported from the Indian Ocean could be seen in this domain. PISCES results

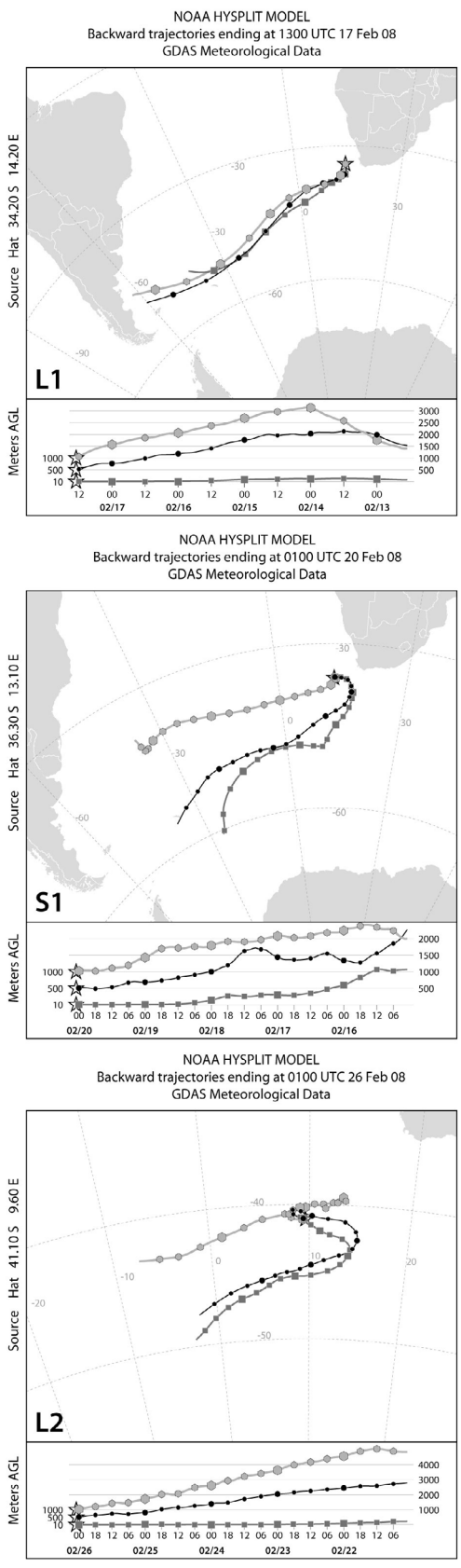

Figure 6. The 5 day back trajectory analysis for heights of 10, 500, and 1000 m, starting from L1, S1, and L2 stations.

also suggest that this source can contribute between 0.1 and 0.3 nmol L^{-1} at stations L2 and L1, respectively (see *Tagliabue et al.* [2009a] for experimental design). As such, these impacts are of similar order to those arising from atmospheric inputs.

[25] Below the surface waters, the AAIW of Indian Ocean origin was observed as deep as 850 m (Figure 2) at the L1 and S1 stations. Those water masses could also be impacted by the African eastern and southern continental slopes, explaining higher DFe concentrations at these subtropical stations (0.6–0.7 nmol L^{-1}) than southerly (<0.5 nmol L^{-1} in the ACC domain). Particles largely dominated the Fe pool in the subtropical domain and particularly at the L1 station in the UCDW and southward slope NADW current. High particle concentrations in the vicinity of the margins have already been observed [*Löscher et al.*, 1997; *Elrod et al.*, 2004; *Lam and Bishop*, 2008]. The decrease in Fe_{app} concentrations from L1 to L2 also agrees with this continental source.

[26] At the S1 station, in the AABW, high DFe values (1.15 and 1.58 nmol L^{-1}) were observed. The water mass at the bottom of the Cape Basin indeed originates from the Weddell Sea and likely transited through fractures in the MAR. Such a mechanism of Fe enrichment at the bottom of the water column was already observed by *Sedwick et al.* [1997] and *Laës et al.* [2003] in the Australian sub-Antarctic region and in the eastern North Atlantic waters, respectively.

4.1.2. ACC Domain (Stations S2, L3, L4, S3, L5, L6, S4, and L7)

[27] The decrease in DFe concentrations from the subtropical domain to the ACC could be due to lower Fe inputs. In the ACC region, the NOAA HYSPLIT model did not suggest any air mass coming from Patagonia or southern Africa during the 5 day period before sampling. The main source of Fe may thus be advection of water masses from the west through the ACC, enriched by Fe from the sediments of the Antarctic Peninsula, South America margin, and/or South Georgia Islands [*Arhan et al.*, 2002; *Löscher et al.*, 1997; *Croot et al.*, 2004; *Korb et al.*, 2004]. Mean water velocities across the ACC have been estimated in the Drake Passage between 2004 and 2007 to be on the order of 16.7 ± 0.2 cm s^{-1} [*Cunningham and Pavic*, 2007]. Estimates of the median advection time for these water masses using outputs of a global ocean general circulation model (ORCA05) and a Lagrangian quantitative diagnostic (ARIANE, http://stockage.univ-brest.fr/~grima/Ariane/ariane.html [*Blanke et al.*, 2006]) suggest a mean transit time of 2 years with a minimum value of 1 year. The residence time of DFe is on the order of days to months in surface waters and of 15–40 years in deep waters [*de Baar and de Jong*, 2001; *Croot et al.*, 2004; *Sarthou et al.*, 2003]. The imprint of Fe coming from South America, the Antarctic Peninsula, and the South Georgia Islands is thus more likely to be seen in the deep waters than in the surface ones. Moreover, the lowest Fe_{app} concentrations of the section were found in the ACC domain, suggestive of no major transport of particulate lithogenic Fe to our study area. *Ridame and Guieu* [2002] calculated settling velocities in seawater of 0.05 to ~18 m d^{-1} for particles from 1 to 20 μm. In 1 year, large particles would thus settle down to the bottom and not reach our study area. However, small particles weathered close to South America and dissolved during the transport to the Greenwich meridian could explain the deep

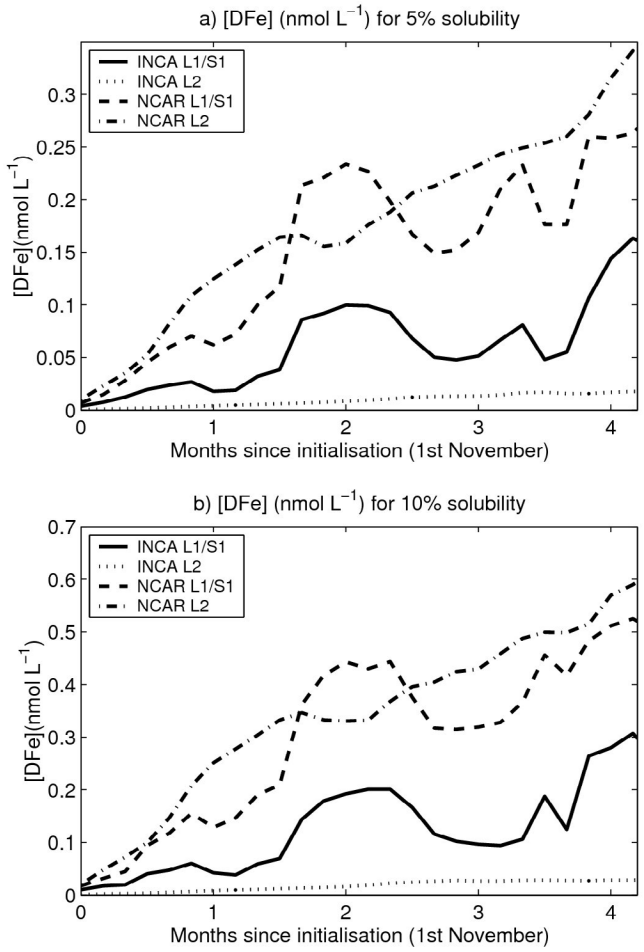

Figure 7. Modeled surface accumulation of dissolved iron (nmol L^{-1}) from 1 November, considering only surface flux processes based on NCAR or INCA dust climatologies, using a 3.5% Fe content and either a (a) 5% Fe solubility or a (b) 10% Fe solubility. Physical advection and diffusion are obtained by an adjusted model configuration (SAfE [*Penven et al.*, 2006]).

DFe concentrations observed in this domain. In deep waters close to the MAR, high values of DFe suggest hydrothermal inputs [*Boyle and Jenkins*, 2008; *Bennett et al.*, 2008; *Tagliabue et al.*, 2010], and high Fe_{app} concentrations measured at the bottom of S2 and S3 are in accordance with slope currents of AABW observed near the oceanic ridge [*Gladyshev et al.*, 2008].

[28] At station L6 located in the PF, an increase in the surface DFe concentrations was observed with values higher than 0.2 nmol L^{-1}. The polar frontal region of the ACC is characterized by a rapid eastward flowing jet. With a velocity of 25 cm s^{-1} [*Cunningham and Pavic*, 2007; *Arhan et al.*, 2002], a mean transit time of 1.3 years with a minimum value of 8 months was calculated. This imprint is thus likely to be seen in surface waters. Besides, active upwelling and eddy diffusion caused by vigorous wind and high deep DFe concentrations (0.6–1.1 nmol L^{-1}) are supposed to supply Fe to surface waters of the polar front [*Löscher et al.*, 1997]. Considering the same approach as *Löscher et al.* [1997], we calculated the upwelled and diffusive fluxes. This leads to a total upward flux of 1.7×10^{-12} mol Fe m^{-2} s^{-1}, similar to previous values [*Löscher et al.*, 1997; *Croot et al.*, 2004] and largely dominated by the advective flux.

4.1.3. Weddell Sea Gyre (Station S5)

[29] This region was characterized by low DFe concentrations and high Fe_{app} concentrations. The phytoplankton in this area was in a growing stage [*Le Moigne et al.*, 2009], which can explain low values of DFe and high concentrations of biogenic particulate Fe. Horizontal advection of lithogenic particles from the west could also explain the high Fe_{app} values at S5. The Weddell-Scotia confluence (WSC) is indeed the largest productive area in the Southern Ocean [*Kahru et al.*, 2007] because of Fe inputs from the Weddell Sea [*Nolting et al.*, 1991]. *Orsi et al.* [1993] observed the physical WSC signal as far as 22°E. Finally, icebergs, which we observed in this region, can be a local source of Fe in surface waters [*Löscher et al.*, 1997].

4.2. Distribution of SFe and CFe

[30] The study of the different Fe sources is of importance to understand how this essential micronutrient may affect primary production in the Southern Ocean. However, its impact on phytoplankton is related to its bioavailability, and DFe is not as bioavailable as previously thought. A significant part of this pool is indeed present under colloidal form [*Wu et al.*, 2001]. Colloids, in particular when older than 15 days, have been shown to be less available than SFe [*Chen and Wang*, 2001]. However, open ocean data on these fractions are lacking to improve our understanding of the Fe cycle. The following paragraphs discuss the distribution of SFe and CFe along the BONUS-GoodHope transect and further explores the interactions between those two pools.

[31] No statistically significant correlation between DFe and SFe was observed ($R^2 = 0.35$, $n = 48$, $p = 0.6$; data not shown). Because CFe is calculated using DFe values, auto-correlation prevents us from examining any relationship between DFe and CFe. Different hypotheses, which are not exclusive, can be formulated to explain CFe and SFe distributions.

[32] 1. The first hypothesis is colloidal aggregation and vertical export of CFe in the water column through scavenging. Fe_{app}, DFe, and CFe concentrations observed in the upper 120 m (except at station S1; see below) presented minimum values at the same depths, suggesting that Fe is not simply partitioned between the dissolved and the particulate fractions. The same observation was reported in some studies and was attributed to vertical export of Fe through scavenging [*Sedwick et al.*, 2005; *Sarthou et al.*, 2007]. Here, colloidal aggregation followed by sinking could thus be an explanation for the CFe minimum in surface waters and the increase in CFe concentrations with depth.

[33] 2. The solubility of Fe is related to the concentrations of soluble and colloidal ligands. *Liu and Millero* [2002] determined a Fe (III) solubility of 0.5 nmol L^{-1} in 0.02 μm of filtered seawater and of 11 pmol L^{-1} in 0.7 mol L^{-1} NaCl (S = 36, T = 5°C, and pH = 8). They concluded that the difference between these two values was due to the presence of soluble Fe-binding organic ligands in seawater. At station S1, located in the subtropical domain, both CFe and SFe concentrations were high (0.2 nmol L^{-1} at 30 m for CFe, 0.4–0.6 nmol L^{-1} in the upper 1500 m for SFe) compared to the concentrations in the other domains of the section

(<0.07 nmol L^{-1} for CFe in surface waters, 0.1–0.4 nmol L^{-1} in the upper 1500 m for SFe). The difference between the microbial planktonic communities may explain the difference between the subtropical domain and the other ones. Numerous studies have shown that prokaryotes (heterotrophic bacteria or cyanobacteria) produce soluble organic molecules such as siderophores that bind Fe and make it more available [*Reid and Butler*, 1991; *Wilhelm and Trick*, 1994; *Butler*, 1998; *Mawji et al.*, 2008]. Unfortunately, during the BONUS-GoodHope cruise, no data on heterotrophic bacteria activity were available to assess the hypothesis of a ligand production by these species. However, at station S1, a bloom in a senescent stage dominated by cyanobacteria was observed (J. Ras and H. Claustre, personal communication, 2009). It could induce a high concentration of siderophores. The senescent stage of the bloom also implies that colloidal ligands such as porphyrines or transparent exopolymer particles may have been released during cell lysis or grazing [*Rue and Bruland*, 1995; *Rue and Bruland*, 1997; *Leppard*, 1997]. It could explain the elevated CFe concentrations measured in the surface waters at the S1 station. Another explanation is the advection of water masses enriched with ligands from continental origin through the Agulhas Current, together with Fe (see section 4.1.1).

[34] 3. The third hypothesis involves biological uptake of the CFe and/or SFe with a subsequent exchange between CFe and SFe. Given that SFe concentrations in surface waters are not depleted, whereas CFe are (except at station S1), our results suggest that CFe may be used for uptake by phytoplankton. Possible mechanisms of CFe uptake are biological reduction at the cell surface [*Maldonado and Price*, 2000, 2001] or direct ingestion [*Barbeau et al.*, 1996]. Some studies have demonstrated the bioavailability of CFe [*Kuma et al.*, 2000; *Chen and Wang*, 2001], especially freshly precipitated colloids (<15 d [*Chen and Wang*, 2001]). However, given that DFe in the ACC domain is suspected to come from the Antarctic Peninsula, South America, and/or the South Georgia Islands, and that the transport time is of 1–2 years, colloids would be aged and may not be easily assimilated. An assimilation of SFe followed by a rapid exchange between the colloidal and the soluble iron could occur [*Wells*, 2003; *Morel et al.*, 2008].

5. Conclusion

[35] The study of the Fe speciation along the BONUS-GoodHope section provides information on the distribution and the sources of Fe in the Atlantic sector of the Southern Ocean.

[36] Dust inputs coming from Patagonia and southern Africa (followed by advection of water masses) seem to be an important source explaining the high Fe_{app} and DFe concentrations observed in surface waters within the subtropical domain. It is encouraging that despite the great differences between ROMS-SAfE and PISCES (in terms of model complexity), their overall conclusions regarding the importance of dust Fe are similar. However, large uncertainties and unknowns persist on the estimation of dust fluxes to the open ocean [*Wagener et al.*, 2008]. The estimation of Fe deposition fluxes in remote areas and of the solubility of these aerosols have to be improved to better constrain this important source of Fe to the open ocean. Inputs of lithogenic Fe transported by slope currents near the African continental margin is an additional explanation to the high DFe and Fe_{app} concentrations observed in the subtropical domain. This process of Fe enrichment is also observed at the bottom of the stations located near the ridge in the ACC domain. Moreover, the ACC domain is characterized by strong currents that can transport Fe from the Drake Passage, the Antarctic Peninsula, and/or the South Georgia Islands. An estimated upwelling flux of 1.7×10^{-12} mol Fe m^{-2} s^{-1} in the polar frontal region was similar to previous values [*Löscher et al.*, 1997; *Croot et al.*, 2004] and could explain the higher values observed in surface waters of the L6 station. Lateral advection of the WSC, continental shelf sediments or melting icebergs could be the source of Fe_{app} south of the SBdy. Hydrothermal inputs could also contribute to some local enrichment of DFe in deep waters.

[37] SFe exhibited the same vertical profiles as samples collected in the Atlantic Ocean [*Wu et al.*, 2001; *Bergquist et al.*, 2007], except in the subtropical domain. Organic ligands released by cyanobacteria and/or advected through the Agulhas Current could explain higher SFe and CFe values observed in this domain. Colloidal aggregation and sinking of CFe, and assimilation of SFe followed by a rapid exchange between the colloidal and the soluble Fe, are also suspected.

[38] More studies on Fe speciation in the soluble and colloidal fractions need to be performed, both in situ and in laboratory process studies, to better constrain the question of the bioavailability of Fe. This would aid further developments of models that aim to include Fe speciation and its effect on bioavailability [*Tagliabue et al.*, 2009b].

[39] **Acknowledgments.** We are grateful to Sabrina Speich, the chief scientist; Frank Dehairs, the cochief scientist; and the captain and the crew of the R.V. Marion Dufresne for their support onboard. This work was supported by the Institut National des Sciences de L'Univers of the Centre National de la Recherche Scientifique, the French Polar Institute (Institut Polaire Emile Victor), the French Research Institute for Exploitation of the Sea, and the Agence National de la Recherche. We thank Alex Baker and Edward Sholkovitz for their comments and Eric Roy and Eric Achterberg for their insightful reviews that improved this manuscript. We acknowledge the Go-Flo sampling team: J. Bown, M. Boyé, F. Lacan, A. Radic, and B. Wake.

References

Arhan, M., A. Naveira Garabato, K. Heywood, and D. Stevens (2002), The Antarctic Circumpolar Current between the Falkland Islands and south Georgia, *J. Phys. Oceanogr.*, *32*(6), 1914–1931, doi:10.1175/1520-0485(2002)032<1914:TACCBT>2.0.CO;2.

Arhan, M., H. Mercier, and Y. Park (2003), On the deep water circulation of the eastern South Atlantic Ocean, *Deep Sea Res. Part I*, *50*(7), 889–916, doi:10.1016/S0967-0637(03)00072-4.

Aumont, O., L. Bopp, and M. Schulz (2008), What does temporal variability in aeolian dust deposition contribute to sea-surface iron and chlorophyll distributions?, *Geophys. Res. Lett.*, *35*, L07607, doi:10.1029/2007GL031131.

Baker, A. R., T. D. Jickells, M. Witt, and K. L. Linge (2006), Trends in the solubility of iron, aluminum, manganese and phosphorus in aerosol collected over the Atlantic Ocean, *Mar. Chem.*, *98*, 43–58, doi:10.1016/j.marchem.2005.06.004.

Barbeau, K., J. W. Moffett, D. A. Caron, P. L. Croot, and D. L. Erdner (1996), Role of protozoan grazing in relieving iron limitation of phytoplankton, *Nature*, *380*, 61–64, doi:10.1038/380061a0.

Bennett, S., E. Achterberg, D. Connelly, P. Statham, G. Fones, and C. German (2008), The distribution and stabilisation of dissolved Fe in deep-sea hydrothermal plumes, *Earth Planet. Sci. Lett.*, *270*(3–4), 157–167, doi:10.1016/j.epsl.2008.01.048.

Bergquist, B. A., J. Wu, and E. A. Boyle (2007), Variability in oceanic dissolved iron is dominated by the colloidal fraction, *Geochim. Cosmochim. Acta*, *71*, 2960–2974, doi:10.1016/j.gca.2007.03.013.

Blain, S., et al. (2007), Effect of natural iron fertilization on carbon sequestration in the Southern Ocean, *Nature*, *446*, 1070–1074, doi:10.1038/nature05700.

Blanke, B., M. Arhan, and S. Speich (2006), Salinity changes along the upper limb of the Atlantic thermohaline circulation, *Geophys. Res. Lett.*, *33*, L06609, doi:10.1029/2005GL024938.

Boebel, O., J. Lutjeharms, C. Schmid, W. Zenk, T. Rossby, and C. Barron (2003), The Cape Cauldron: A regime of turbulent inter-ocean exchange, *Deep Sea Res. Part II*, *50*, 57–86, doi:10.1016/S0967-0645(02)00379-X.

Boyd, P. W., et al. (2000), A mesoscale phytoplankton bloom in the polar Southern Ocean stimulated by iron fertilization, *Nature*, *407*, 695–702, doi:10.1038/35037500.

Boyd, P. W., T. Jickells, C. Law, S. Blain, E. Boyle, K. Buesseler, K. Coale, J. Cullen, H. De Baar, and M. Follows (2007), Mesoscale iron enrichment experiments 1993–2005: Synthesis and future directions, *Science*, *315*(5812), 612–617, doi:10.1126/science.1131669.

Boyle, E., and W. Jenkins (2008), Hydrothermal iron in the deep western South Pacific, *Geochim. Cosmochim. Acta*, *72*, A107.

Bruland, K. W., R. P. Franks, G. A. Knauer, and J. H. Martin (1979), Sampling and analytical method for the determination of copper, cadmium, zinc, and nickel at the nanogram per liter level in seawater, *Anal. Chim. Acta*, *105*, 233–245, doi:10.1016/S0003-2670(01)83754-5.

Bucciarelli, E., S. Blain, and P. Tréguer (2001), Iron and manganese in the wake of the Kerguelen Islands (Southern Ocean), *Mar. Chem.*, *73*(1), 21–36, doi:10.1016/S0304-4203(00)00070-0.

Butler, A. (1998), Acquisition and utilization of transition metal ions by marine organisms, *Science*, *281*, 207–209, doi:10.1126/science.281.5374.207.

Chen, M., and W.-X. Wang (2001), Bioavailability of natural colloid-bound iron to marine plankton: Influences of colloidal size and aging, *Limnol. Oceanogr.*, *46*(8), 1956–1967, doi:10.4319/lo.2001.46.8.1956.

Chen, M., R. C. H. Dei, W.-X. Wang, and L. Guo (2003), Marine diatom uptake of iron bound with natural colloids of different origins, *Mar. Chem.*, *81*(3–4), 177–189, doi:10.1016/S0304-4203(03)00032-X.

Chever, F., G. Sarthou, E. Bucciarelli, S. Blain, and A. R. Bowie (2010), An iron budget during the natural iron fertilisation experiment KEOPS (Kerguelen Islands, Southern Ocean), *Biogeosciences*, *7*, 455–468, doi:10.5194/bg-7-455-2010.

Coale, K. H., et al. (2004), Southern Ocean iron enrichment experiment: Carbon cycling in high- and low-Si waters, *Science*, *304*(5669), 408–414, doi:10.1126/science.1089778.

Croot, P. L., K. Andersson, M. Ozturk, and D. R. Turner (2004), The distribution and speciation of iron along 6°E in the Southern Ocean, *Deep Sea Res. Part I*, *51*(22–24), 2857–2879.

Cullen, J. T., B. A. Bergquist, and J. W. Moffett (2006), Thermodynamic characterization of the partitioning of iron between soluble and colloidal species in the Atlantic Ocean, *Mar. Chem.*, *98*, 295–303, doi:10.1016/j.marchem.2005.10.007.

Cunningham, S. A., and M. Pavic (2007), Surface geostrophic currents across the Antarctic circumpolar current in Drake Passage from 1992 to 2004, *Prog. Oceanogr.*, *73*(3–4), 296–310, doi:10.1016/j.pocean.2006.07.010.

de Baar, H. J. W., and J. T. M. de Jong (2001), Distributions, sources and sinks of iron in seawater, in *Biogeochemistry of Iron in Seawater*, edited by D. R. Turner and K. A. Hunter, pp. 123–253, Wiley, Baltimore, Md.

de Baar, H. J. W., J. T. M. de Jong, R. F. Nolting, K. R. Timmermans, M. A. van Leeuwe, U. Bathman, M. R. van der Loeff, and J. Sildam (1999), Low dissolved Fe and the absence of diatom blooms in remote Pacific waters of the Southern Ocean, *Mar. Chem.*, *66*, 1–34, doi:10.1016/S0304-4203(99)00022-5.

de Jong, J. T. M., P. L. Croot, and H. J. W. de Baar (1999), Distribution of iron in the surface and deep waters of the Southern Ocean along 20°E, *Eos Trans. AGU*, *80*(49), 161.

Desboeufs, K. V., A. Sifikitis, R. Losno, J. L. Colin, and P. Ausset (2005), Trace metal dissolution and solubility from mineral particles, *Chemosphere*, *58*, 195–203, doi:10.1016/j.chemosphere.2004.02.025.

Duce, R., and N. Tindale (1991), Atmospheric transport of iron and its deposition in the ocean, *Limnol. Oceanogr.*, *36*, 1715–1726, doi:10.4319/lo.1991.36.8.1715.

Ducet, N., P. Y. Le Traon, and G. Reverdin (2000), Global high-resolution mapping of ocean circulation from TOPEX/POSEIDON and ERS-1 and -2, *J. Geophys. Res.*, *105*(C8), 19,477–19,498.

Elrod, V. A., W. M. Berelson, K. H. Coale, and K. S. Johnson (2004), The flux of iron from continental shelf sediments: A missing source for global budgets, *Geophys. Res. Lett.*, *31*, L12307, doi:10.1029/2004GL020216.

Erickson, D., III, J. Hernandez, P. Ginoux, W. Gregg, C. McClain, and J. Christian (2003), Atmospheric iron delivery and surface ocean biological activity in the Southern Ocean and Patagonian region, *Geophys. Res. Lett.*, *30*(12), 1609, doi:10.1029/2003GL017241.

Gassó, S., and A. Stein (2007), Does dust from Patagonia reach the sub-Antarctic Atlantic Ocean?, *Geophys. Res. Lett.*, *34*, L01801, doi:10.1029/2006GL027693.

Gladyshev, S., M. Arhan, A. Sokov, and S. Speich (2008), A hydrographic section from South Africa to the southern limit of the Antarctic Circumpolar Current at the Greenwich meridian, *Deep Sea Res. Part I*, *55*, 1284–1303, doi:10.1016/j.dsr.2008.05.009.

Gledhill, M., and C. M. G. van den Berg (1994), Determination of complexation of iron(III) with natural organic complexing ligands in seawater using cathodic stripping voltammetry, *Mar. Chem.*, *47*, 41–54, doi:10.1016/0304-4203(94)90012-4.

Gordon, A. L., R. F. Weiss Jr., W. M. Smethie, and M. J. Warner (1992), Thermocline and intermediate water communication between the South Atlantic and Indian oceans, *J. Geophys. Res.*, *97*(C5), 7223–7240, doi:10.1029/92JC00485.

Jickells, T., and L. J. Spokes (2001), Atmospheric iron inputs to the oceans, in *The Biogeochemistry of Iron in Seawater*, edited by D. R. Turner and K. A. Hunter, pp. 85–121, Wiley, Baltimore, Md.

Jickells, T. D., et al. (2005), Global iron connections between desert dust, ocean biogeochemistry, and climate, *Science*, *308*, 67–71, doi:10.1126/science.1105959.

Johnson, K., et al. (2007), Developing standards for dissolved iron in seawater, *Eos Trans. AGU*, *88*(11), 131–132, doi:10.1029/2007EO110003.

Kahru, M., B. Mitchell, S. Gille, C. Hewes, and O. Holm-Hansen (2007), Eddies enhance biological production in the Weddell-Scotia Confluence of the Southern Ocean, *Geophys. Res. Lett.*, *34*, L14603, doi:10.1029/2007GL030430.

Klatt, O., E. Fahrbach, M. Hoppema, and G. Rohardt (2005), The transport of the Weddell Gyre across the Prime meridian, *Deep Sea Res. Part II*, *52*, 513–528, doi:10.1016/j.dsr2.2004.12.015.

Korb, R., M. Whitehouse, and P. Ward (2004), SeaWIFS in the Southern Ocean: Spatial and temporal variability in phytoplankton biomass around south Georgia, *Deep Sea Res. Part II*, *51*(1–3), 99–116, doi:10.1016/j.dsr2.2003.04.002.

Kuma, K., J. Tanaka, K. Matsunaga, and K. Matsunaga (2000), Effect of hydroxamate ferrisiderophore complex (ferrichrome) on iron uptake and growth of a coastal marine diatom, *Chaetoceros sociale*, *Limnol. Oceanogr.*, *45*(6), 1235–1244, doi:10.4319/lo.2000.45.6.1235.

Laës, A., S. Blain, P. Laan, E. P. Achterberg, G. Sarthou, and H. J. W. de Baar (2003), Deep dissolved iron profiles in the eastern North Atlantic in relation to water masses, *Geophys. Res. Lett.*, *30*(17), 1902, doi:10.1029/2003GL017902.

Lam, P. J., and K. B. Bishop (2008), The continental margin is a key source of iron to the HNLC North Pacific Ocean, *Geophys. Res. Lett.*, *35*, L07608, doi:10.1029/2008GL033294.

Lancelot, C., A. de Montely, H. Goosse, S. Becquevort, V. Schoemann, B. Pasquer, and M. Vancoppenolle (2009), Spatial distribution of the iron supply to phytoplankton in the Southern Ocean: A model study, *Biogeosciences*, *6*, 2861–2878, doi:10.5194/bg-6-2861-2009.

Landing, W. M., and R. T. Powell (1998), Vertical profiles of dissolved and particulate iron in the southern and equatorial Atlantic: Relationships between atmospheric deposition, biogeochemical cycling, and inorganic scavenging, *Eos Trans. AGU*, *79*(1), 137.

Le Moigne, F., M. Boye, A. Masson, and A. Guenegues (2009), The nutrients and chlorophyll status of the southern ocean in the Atlantic sector during the international polar year poster session, paper presented at Aquatic Sciences Meeting, Am. Soc. Limnol. Oceanogr., Nice, France.

Leppard, G. (1997), Colloidal organic fibrils of acid polysaccharides in surface waters: Electron-optical characteristics, activities and chemical estimates of abundance, *Colloids Surf. A*, *120*(1–3), 1–15, doi:10.1016/S0927-7757(96)03676-X.

Liu, X., and F. J. Millero (2002), The solubility of iron in seawater, *Mar. Chem.*, *77*(1), 43–54, doi:10.1016/S0304-4203(01)00074-3.

Löscher, B. M., H. J. W. de Baar, J. T. M. de Jong, C. Veth, and F. Dehairs (1997), The distribution of Fe in the Antarctic Circumpolar Current, *Deep Sea Res. Part II*, *44*, 143–187, doi:10.1016/S0967-0645(96)00101-4.

Lutjeharms, J., and R. van Ballegooyen (1988), The retroflection of the Agulhas Current, *J. Phys. Oceanogr.*, *18*, 1570–1583, doi:10.1175/1520-0485(1988)018<1570:TROTAC>2.0.CO;2.

Mahowald, N., K. Kohfeld, M. Hansson, Y. Balkanski, S. P. Harrison, I. C. Prentice, M. Schulz, and H. Rodhe (1999), Dust sources and deposition during the last glacial maximum and current climate: A comparison of model results with paleodata from ice cores and marine sediments, *J. Geophys. Res.*, *104*, 15,895–15,916, doi:10.1029/1999JD900084.

Mahowald, N., D. R. Muhs, S. Levis, P. J. Rasch, M. Yoshioka, C. S. Zender, and C. Luo (2006), Change in atmospheric mineral aerosols in response to climate: Last glacial period, preindustrial, modern, and

doubled carbon dioxide climates, *J. Geophys. Res.*, *111*, D10202, doi:10.1029/2005JD006653.
Maldonado, M. T., and N. M. Price (2000), Nitrate regulation of Fe reduction and transport by Fe-limited *Thalassiosira oceanica*, *Limnol. Oceanogr.*, *45*(4), 814–826, doi:10.4319/lo.2000.45.4.0814.
Maldonado, M. T., and N. M. Price (2001), Reduction and transport of organically bound iron by *Thalassiosira oceanica* (Bacillariophyceae), *J. Phycol.*, *37*(2), 298–310, doi:10.1046/j.1529-8817.2001.037002298.x.
Martin, J. H., R. M. Gordon, and S. E. Fitzwater (1990), Iron in Antarctic waters, *Nature*, *345*, 156–158, doi:10.1038/345156a0.
Mawji, E., M. Gledhill, J. Milton, G. Tarran, S. Ussher, A. Thompson, G. Wolff, P. Worsfold, and E. Achterberg (2008), Hydroxamate siderophores: Occurrence and importance in the Atlantic Ocean, *Environ. Sci. Technol.*, *42*(23), 8675–8680, doi:10.1021/es801884r.
Meredith, M. P., R. A. Locarnini, K. A. Van Scoy, A. J. Watson, K. J. Heywood, and B. A. King (2000), On the sources of Weddell Gyre Antarctic Bottom Water, *J. Geophys. Res.*, *105*(C1), 1093–1104, doi:10.1029/1999JC900263.
Meskhidze, N., A. Nenes, W. Chameides, C. Luo, and N. Mahowald (2007), Atlantic Southern Ocean productivity: Fertilization from above or below?, *Global Biogeochem. Cycles*, *21*, GB2006, doi:10.1029/2006GB002711.
Morel, F. M. M., A. B. Kustka, and Y. Shaked (2008), The role of unchelated Fe in the iron nutrition of phytoplankton, *Limnol. Oceanogr.*, *53*(1), 400–404.
Nishioka, J., S. Takeda, and C. S. Wong (2001), Change in the concentrations of iron in different size fractions during a phytoplankton bloom in controlled ecosystem enclosures, *J. Exp. Mar. Biol. Ecol.*, *258*, 237–255, doi:10.1016/S0022-0981(01)00219-2.
Nishioka, J., S. Takeda, H. de Baar, P. Croot, M. Boye, P. Laan, and K. Timmermans (2005), Changes in the concentration of iron in different size fractions during an iron enrichment experiment in the open Southern Ocean, *Mar. Chem.*, *95*(1–2), 51–63, doi:10.1016/j.marchem.2004.06.040.
Nolting, R. F., H. J. W. de Baar, A. J. Bennekom, and A. Masson (1991), Cadmium, copper and iron in the Scotia Sea, Weddel Sea and Weddel/Scotia Confluence (Antarctica), *Mar. Chem.*, *35*, 219–243, doi:10.1016/S0304-4203(09)90019-6.
Obata, H., H. Karatani, and E. Nakayama (1993), Automated determination of iron in seawater by chelating resin concentration and chemiluminescence, *Anal. Chem.*, *65*, 1524–1528, doi:10.1021/ac00059a007.
Orsi, A. H., W. D. Nowlin Jr., and T. Whitworth III (1993), On the circulation and stratification of the Weddell Gyre, *Deep Sea Res. Part I*, *40*, 169–203, doi:10.1016/0967-0637(93)90060-G.
Penven, P., J. Lutjeharms, and P. Florenchie (2006), Madagascar: A pacemaker for the Agulhas Current system?, *Geophys. Res. Lett.*, *33*, L17609, doi:10.1029/2006GL026854.
Piketh, S., R. Swap, W. Maenhaut, H. Annegarn, and P. Formenti (2002), Chemical evidence of long-range atmospheric transport over southern Africa, *J. Geophys. Res.*, *107*(D24), 4817, doi:10.1029/2002JD002056.
Pollard, R. T., et al. (2009), Southern Ocean deep-water carbon export enhanced by natural iron fertilization, *Nature*, *457*, 577–580, doi:10.1038/nature07716.
Reid, J. L. (1989), On the total geostrophic circulation of the South Atlantic Ocean: Flow patterns, tracers, and transports, *Prog. Oceanogr.*, *23*, 149–244, doi:10.1016/0079-6611(89)90001-3.
Reid, R. T., and A. Butler (1991), Investigation of the mechanism of iron acquisition by the marine bacterium *Alteromonas luteoviolaceus*: Characterization of siderophores production, *Limnol. Oceanogr.*, *36*, 1783–1792, doi:10.4319/lo.1991.36.8.1783.
Ridame, C., and C. Guieu (2002), Saharan input of phosphorus to the oligotrophic water of the open western Mediterranean, *Limnol. Oceanogr.*, *47*(3), 856–869, doi:10.4319/lo.2002.47.3.0856.
Rue, E. L., and K. W. Bruland (1995), Complexation of iron(III) by natural organic ligands in the Central North Pacific as determined by a new competitive ligand equilibration/adsorptive cathodic stripping voltammetric method, *Mar. Chem.*, *50*(1–4), 117–138, doi:10.1016/0304-4203(95)00031-L.
Rue, E. L., and K. W. Bruland (1997), The role of organic complexation on ambient iron chemistry in the equatorial Pacific Ocean and the response of a mesoscale iron addition experiment, *Limnol. Oceanogr.*, *42*(5), 901–910, doi:10.4319/lo.1997.42.5.0901.
Sarthou, G., et al. (2003), Atmospheric iron deposition and sea-surface dissolved iron concentrations in the eastern Atlantic Ocean, *Deep Sea Res. Part I*, *50*(10–11), 1339–1352, doi:10.1016/S0967-0637(03)00126-2.
Sarthou, G., A. R. Baker, J. Kramer, P. Laan, A. Laës, S. Ussher, E. P. Achtenberg, H. J. W. de Baar, K. R. Timmermans, and S. Blain (2007), Influence of atmospheric inputs on the iron distribution in the subtropical north-east Atlantic Ocean, *Mar. Chem.*, *104*, 186–202, doi:10.1016/j.marchem.2006.11.004.
Sedwick, P. N., and G. R. DiTullio (1997), Regulation of algal blooms in Antarctic shelf waters by the release of iron from melting sea ice, *Geophys. Res. Lett.*, *24*(20), 2515–2518, doi:10.1029/97GL02596.
Sedwick, P. N., P. R. Edwards, D. J. Mackey, F. B. Griffiths, and J. S. Parslow (1997), Iron and manganese in surface waters of the Australian subantarctic region, *Deep Sea Res. Part I*, *44*, 1239–1253.
Sedwick, P. N., T. M. Church, A. R. Bowie, C. M. Marsay, S. J. Ussher, K. M. Achilles, P. J. Lethaby, R. J. Johnson, M. M. Sarin, and D. J. McGillicuddy (2005), Iron in the Sargasso Sea (Bermuda Atlantic time-series study region) during summer: Eolian imprint, spatiotemporal variability, and ecological implications, *Global Biogeochem. Cycles*, *19*, GB4006, doi:10.1029/2004GB002445.
Sedwick, P. N., A. R. Bowie, and T. W. Trull (2008), Dissolved iron in the Australian sector of the Southern Ocean (CLIVAR SR3 section): Meridional and seasonal trends, *Deep Sea Res. Part I*, *55*, 911–925, doi:10.1016/j.dsr.2008.03.011.
Smith, K., Jr., B. Robison, J. Helly, R. Kaufmann, H. Ruhl, T. Shaw, B. Twining, and M. Vernet (2007), Free-drifting icebergs: Hot spots of chemical and biological enrichment in the Weddell Sea, *Science*, *317*(5837), 478–482, doi:10.1126/science.1142834.
Sunda, W. G. (1988–1989), Trace metal interactions with marine phytoplankton, *Biol. Oceanogr.*, *6*, 411–442.
Tagliabue, A., L. Bopp, and O. Aumont (2009a), Evaluating the importance of atmospheric and sedimentary iron sources to Southern Ocean biogeochemistry, *Geophys. Res. Lett.*, *36*, L13601, doi:10.1029/2009GL038914.
Tagliabue, A., L. Bopp, O. Aumont, and K. R. Arrigo (2009b), Influence of light and temperature on the marine iron cycle: From theoretical to global modeling, *Global Biogeochem. Cycles*, *23*, GB2017, doi:10.1029/2008GB003214.
Tagliabue, A., et al. (2010), Hydrothermal contribution to the oceanic dissolved iron inventory, *Nat. Geosci.*, *3*, 252–256, doi:10.1038/ngeo818.
van Ballegooyen, R. C., M. L. Gründlingh, and J. R. E. Lutjeharms (1994), Eddy fluxes of heat and salt from the southwest Indian Ocean into the southeast Atlantic Ocean: A case study, *J. Geophys. Res.*, *99*(C7), 14,053–14,070, doi:10.1029/94JC00383.
Wagener, T., C. Guieu, R. Losno, S. Bonnet, and N. Mahowald (2008), Revisiting atmospheric dust export to the southern hemisphere ocean: Biogeochemical implications, *Global Biogeochem. Cycles*, *22*, GB2006, doi:10.1029/2007GB002984.
Wells, M. L. (2003), The level of iron enrichment required to initiate diatom blooms in HNLC waters, *Mar. Chem.*, *82*, 101–114, doi:10.1016/S0304-4203(03)00055-0.
Whitworth, T., III, and J. W. D. Nowlin (1987), Water masses and currents of the Southern Ocean at the Greenwich meridian, *J. Geophys. Res.*, *92*(C6), 6462–6476, doi:10.1029/JC092iC06p06462.
Wilhelm, S. W., and C. G. Trick (1994), Iron-limited growth in cyanobacteria: Multiple siderophore production is a common response, *Limnol. Oceanogr.*, *39*, 1979–1984, doi:10.4319/lo.1994.39.8.1979.
Wu, J., E. Boyle, W. Sunda, and L.-S. Wen (2001), Soluble and colloidal iron in the oligotrophic North Atlantic and North Pacific, *Science*, *293*, 847–849, doi:10.1126/science.1059251.

M. Arhan, P. Penven, and S. Speich, Laboratoire de Physique des Océans, UMR 6523, IFREMER, CNRS, IRD, UBO, Centre de Brest, BP 70, F-29280 Plouzane, France.
E. Bucciarelli, F. Chever, and G. Sarthou, LEMAR, UMR 6539, Université de Brest, CNRS, IRD, UBO, IUEM, Technopôle Brest Iroise, Place Nicolas Corpernic, F-29280 Plouzane, France. (eva.bucciarelli@univ-brest.fr; fanny.chever@univ-brest.fr)
A. Tagliabue, LSCE, UMR 1572, IPSL, CEA, CNRS, UVSQ, Orme des Merisiers, F-91191 Gif-sur-Yvette, France.